International Journal of Nanoelectronics and Materials
IJNeaM
ISSN 1985-5761 | E-ISSN 2232-1535

Decision Making Using Analytic Hierarchy Process for Plasmonic Waveguide Simulated by Finite-Difference Eigenmode Method

Amnh S. Hasan[a], Ali A. Alwahib[a,*], Razi J. Al-Azawi[a], Qamar Q. Mohammed[b], Omar S. Dahham[c], Fariza H. Suhailin[d], Ayman M. Hassan[e], Ahmed A. Al-Amiery[f], Makram A. Fakhri[a,**]

[a]*College of Laser and Optoelectronics, University of Technology-Iraq, Baghdad, Iraq*
[b]*College of Control, University of Technology-Iraq, Baghdad, Iraq*
[c]*Department of Chemical Engineering, Faculty of Engineering, University of Baghdad, Baghdad, Iraq*
[d]*Physics Department, Faculty of Science, Universiti Teknologi Malaysia (UTM), 81310 Skudai, Johor Bahru, Malaysia*
[e]*Laser and Optoelectronics Engineering Department, Dijla University College, Baghdad, Iraq*
[f]*Al-Ayen Scientific Research Center, Al-Ayen Iraqi University, AUIQ, P.O. Box: 64004, An Nasiriyah, Thi Qar, Iraq*
**Corresponding author. E-mail: Ali.A.Alwahib@uotechnology.edu.iq, 140009@uotechnology.edu.iq*
***Corresponding author. E-mail: Makram.a.fakhri@uotechnology.edu.iq*

ABSTRACT

The thickness and materials of a plasmonic layer play a vital role in identifying the highest confinement loss. The finite-difference Eigenmode method (FDE) and the Analytic Hierarchy Process were used to analyze plasmonic waveguide layers. FDE was applied to single-plasmonic layers (Au, Ag, and Cu) and multi- plasmonic layers (Au/Ag, Au/Cu). Refractive index variation (1.1, 1.2, and 1.3) are used to study the highest loss, full-width half maximum (FWHM), and Figure of merits (FOM). Three waveguide designs in multi-layer thickness are used (10/30, 20/30, and 30/30) nanometers. The waveguide sensitivity results for the single Ag layer are 112 nm/RIU, higher than Au and Cu, 66 nm/RIU, and 71 nm/RIU respectively. The sensitivity result of multi-layers is 100 nm/RIU for Au/Ag and 47nm/RIU for Au/Cu. The maximum absorption in Au is 257.5 a.u. at a thickness of 30 nm, and FWHM is 35.8 for the same thickness. The best option and priority for the waveguide optical characteristics are found using Analytic Hierarchy Process (AHP) was Au rank #1, and priority was 93%, followed by Ag rank #2 at 91% priority. Au/Cu (10/30) thickness rank #5 is the best option and priority 86% in multi-layers results. To the best of our knowledge, there has yet to be a report for analyzing the multi-layer using FDE. Also, AHP-based plasmonic sensors for single and multi-layer types are yet to be presented.

Keywords: *Waveguide, Plasmonic, Sensor, Thickness, Single layer, Multi-layers*

1. INTRODUCTION

The main job of sensors is gathering information from the environment or fundamental function of a complex systemin in the form of signals. The origin of this signal is optical, by using a sensor it will transform to a measurable signal and then to the system. The evolution in sensor systems made research a critical issue in meeting the demands of modern applications [1, 3]. As technology advances and intelligent systems become more complicated, sensing technologies must become more effective and trustworthy [4-6]. The rapid growth of optical waveguide technologies has recently significantly impacted the current optical electronic industrial, medical devices, and information technology [7-9].

Optical waveguides are classified based on their geometry into three configurations: planar, rectangular, and cylindrical channel [10-12]. Mode structure in Single-mode and multiple modes optical waveguides are also other types of waveguide classification [123-15]. Guidelight between two locations is one of the characteristics of optical waveguides. Optical waveguides sensors have several advantages, including compact size, durability, multichannel sensing, working in very broad wavelength range [16-18]. Light propagation in an optical waveguide in some sensors applications is the principle of the optical sensor work such as plasmonic based sensors [19-21].

Plasmonic interfaces are applied as an option for substantially effective light control techniques for nano sensor applications. Surface plasmons waves are guided waves on the interface; the free electrons at the plasmonic material interface respond collectively to an electromagnetic disturbance and produce these guided waves. Surface plasmons are waves that can be excited by TM-polarized waves and work similarly to the Kretschmann arrangement. For the excitation condition, the wave vector of the surface plasmon should be equal to the wave vector of the incident light [22-24], $k\_x^{pr}=k\_x^{sp}$ where kx^{pr} is the wavevector of incident light and kx^{sp} is the wavevector of surface plasmon, $\boldsymbol{k_x^{sp}} = \sqrt{\left(\frac{\tilde{\varepsilon_1}\tilde{\varepsilon_2}}{\tilde{\varepsilon_1}+\tilde{\varepsilon_2}}\right)}\left(\frac{w}{c}\right)$, and $\boldsymbol{k_x^{pr}} = \frac{w}{c}\sqrt{\boldsymbol{\varepsilon_{pr}}}\,\boldsymbol{sin\theta_{pr}}$) where w is the light frequency, c is the speed of light,ε_1~ and ε_2~ are the dielectric constants of dielectric medium and metal layer, respectively. θ_{pr} is the angle at the boundary between the dielectric (prism) and a metal layer, and ε_{pr} is the dielectric constant of a prism. The SPs are excited by the dielectric waveguide modes; when a waveguide mode reaches the metal layer, it evanescently

penetrates the metal layer and then gets coupled with SP at the external surface of the metal [25-27]. When the propagation constants of both modes are equivalent, this coupling happens. The deployment of the waveguide in SPR sensors facilitates effective control of the properties of light. The coupling strength depends upon the thickness of the metal layer and the interaction length. Thus, as a result, waveguides may be used to create tiny and readily programmable sensors [28-30]. The optical characteristics of waveguides can be set according to the type of applications, for example, materials, size, and design. Selecting the best attributes for any application requires many experiments, and choosing the best result requires an analytic method [31-33].

In 1995 R.D. Harris et al. proposed to design a simple SPR sensor based on a step-index slab waveguide; it used where optimum sensitivity is not required and designed another sensor with a low refractive index of buffer layer [34]. Blow H. Ong et al. in 2007 presented a waveguide SPR sensor with fabricated three different metallic configurations, single-layered Ag and Au, and layers Ag–Au. The experimental result showed that the bimetallic film setup possesses 594 nm/RIU to 1,232 nm/RIU [35]. Satyendra K. et al. in 2016, suggested plasmonic sensor gain and found the sensitivity is~45 μm/RIU; this sensor was built from a polymer channel waveguide. The primary material was 40 nm thick copper coated with a 10 nm thickness of silicon- dioxide [36] and in 2020 M. S. Aruna G. et al. proposed building a small, simple, and efficient self-referenced sensor that detects the unknown analyte using a finite element method with a range of refractive index 1.3 to 1.45 analyte. They found the sensitivity is 38000 nm/RIU with used wavelengths range from 400 to 1800 nm and the thickness of the gold layer is 40 nm [37]. In 2020 Lanting JI et al. suggested fabricating an SPR sensor using the finite difference method. They found that the gold layer's thickness affects the sensor's sensitivity sensor, a thinner gold film gives good sensitivity until certain limits [38].

The analytic Hierarchy Process consists of four steps (1) State the decision, the alternatives, and the standards. (2) Perform pairwise contrasts. (3) Determine each criterion's priority weight. (4) Determine the optimal choice by doing a utility calculation. AHP is a helpful method to make a complex decision when no valuable clear answer is found. Every decision is preceded by a question, for example, what are the most important criteria that make the sensor work in a hot environment. These criteria should be organized into matrix form; each column and row contain a criterion. A practical tool that can be utilized at home, school, or the office is the AHP. It ensures that choice represents values and goals and removes bias from the decision-making process. The AHP can be applied in countless ways; the only restriction is the researcher's imagination.

The study of sensor characteristics based on an analytic (AHP) method, especially for sensors have been applied but still need more investigation. T. Al-Hawari [39] AHP applied an analytic method to select the best temperature sensor among different alternative sensors in a certain industrial application [40] Ahmed F. and Hela M. [41] focused on pairwise comparison automation to remove subjectivity and reduce inconsistency, as well as the use of multi-sensor data fusion to handle conflicting and imperfect data problems. The modified average combination algorithm combines the weighted readings, represented by belief functions, according to the relative relevance (weight) assigned to each sensor piece of data. In 2023 Divya P., and Vandana K. applied AHP for security-aware congestion control in sensor-based networks. A multi-criteria decision-making method has applied as there are many factors responsible for congestion occurrence [39] AHP For plasmonic sensors, has not been presented yet.

In This study, the FDE-AHP plasmonic waveguide sensor is proposed at a wavelength ranging from (200 nm to 1000 nm) by employing a single layer and multi-layers. Based on our survey, using FDE supported by AHP optimized a plasmonic material thickness for high absorption in multi-layers sensor never proposed before.

2. AHP

A correlational approach is essential for the criteria importance by entering criteria correlation [42-45]. The AHP should start with scientific question and the research question of this research paper is, what is the best plasmonic material or alloy can gain the best properties according to Thick, Loss, Resonance, Wavelength, full width half maximum, refractive index, Sensitivity, and Figure of Merit?

Step1: starting from an initial decision matrix, $X = [\xi ij]_{m\times n}$

$$X = \begin{array}{c} \\ A1 \\ A2 \\ Am \end{array} \begin{array}{c} \begin{array}{cccc} C_1 & C_2 & \ldots\ldots. & C_n \end{array} \\ \begin{bmatrix} \xi_{11} & \xi_{12} & \ldots \xi_{1n} \\ \xi_{21} & \xi_{22} & \ldots \xi_{2n} \\ \xi_{m1} & \xi_{m2} & \ldots \xi_{mn} \end{bmatrix}_{m\times n} \end{array} \quad (1)$$

The normalization of matrix elements $X = [\xi_{ij}]_{m\times n}$ is done by applying (2) and (3)

2.1. For Maximizing Criteria

$$\xi_{ij} = \frac{\xi_{ij} - \xi_j^{min}}{\xi_j^{max} - \xi_j^{min}} \quad (2)$$

2.2 For Minimizing Criteria

$$\xi_{IJ=} \frac{\xi_j^{max} - \xi_{ij}}{\xi_j^{max} - \xi_j^{min}} \quad (3)$$

Where

$$\xi_j^{max} = {}^{max}_{j}\{\xi_{1j}, \xi_{2j}, \ldots, \xi_{mj}\};\ \xi_j^{min} = {}^{min}_{j}\{\xi_{1j}, \xi_{2j}, \xi_{mj}\} \quad (4)$$

Upon criterion for normalization of the original decision matrix, all criteria have the same metrics because all elements ξ_{ij} are reduced to interval values [0,1], c_j (j=1,2,...,n) define the standard deviation σ_j, $\chi = [\xi]_{mx}$ and separate the vector $\xi_j = (\xi_{1j}, \xi_{2j,.....}\xi_{mj})$ that contains the values of alternatives A_i $(i = 1,2,\dots,m)$ for the given criterion c_j $(j = 1,2,\dots,m)$ after forming the vector $\xi_j = (\xi_{1j}, \xi_{2j}, \dots .\xi_{mj})$ the matrix was constructed $L = [\iota_{jk}]_{n\times n}$ that contains coefficients of linear correlation of vectors ξ_j *and* ξ_k [46-49].

$$\boldsymbol{\varphi_j} = \sum_{k=1}^{n}(\mathbf{1} - \boldsymbol{\iota_{jk}}) \quad (5)$$

Multiple-criteria approach (AHP) is based on the necessity for complicated issues to be divided into a hierarchical structure of particular parts such as objective (goal), criteria (sub-criteria), and alternatives [50-52].

3. EXPERIMENTAL PART

A lumerical program is a mathematical model containing Maxwell's equations to model waveguide constants and get dependable results. This program simulates the refractive index and thickness for generating plasmonic waves at the metal-dielectric interface. Moreover, the metal used in the structure design was suggested, as shown in Figure 1.

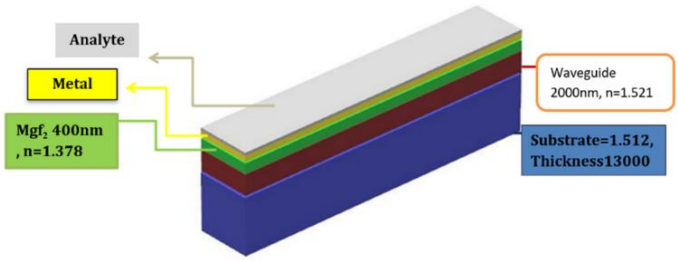

Figure 1. Multi-layers waveguide design.

The configuration of the sensor was done with a Mode simulator by Finite-Difference Eigenmode solver (FDE) to calculate the wavelength resonance and the higher loss. Solver type (1D Y: Z prop) with dimensions that are (y=8000 nm), boundary conditions (metal). Modeling of the structure of sensor contains substrate (13000nm) y span, x span (24000 nm), z span (1000 nm) with refractive index (1.512). Waveguide y span (2000 nm),x span (24000 nm), z span (1000) with refractive index (1.521). Magnesium fluoride buffer layer y span (400 nm),x span (24000 nm),z span (1000 nm) with refractive index (1.378) In conjunction with thin sensing films.

The Palik model simulated a single-layer interface for waveguide metal design that includes gold, silver, and copper at different thicknesses. The maximum loss of each metal was used to change the analyte's refractive index for calculating the waveguide's performance parameter. The performance parameters are sensitivity, Figure of merit (FOM), full width half maximum (FWHM), Resonance wavelength, and highest loss.

In the multi-layers (interfaces) sensor, the design was Au/Ag and Au/Cu simulated using the same model (Palik) and dimensions. In this design, the thickness of gold was 10, 20, and 30 nm under different refractive index (RI) 1.1, 1.2, and 1.3 of the analytes. The optical characteristics of the waveguide were calculated for each Au thickness and RI.

The final work was to estimate the mode profile for wavelength resonance by dimension for FDE solver, x span 24 mm, y span 1 mm and the solver type 2D Z normal, mesh dimension x span 24 mm, y span 1 mm, the distance between every two points in the mesh is 0.01 mm, as shown in Figure 2.

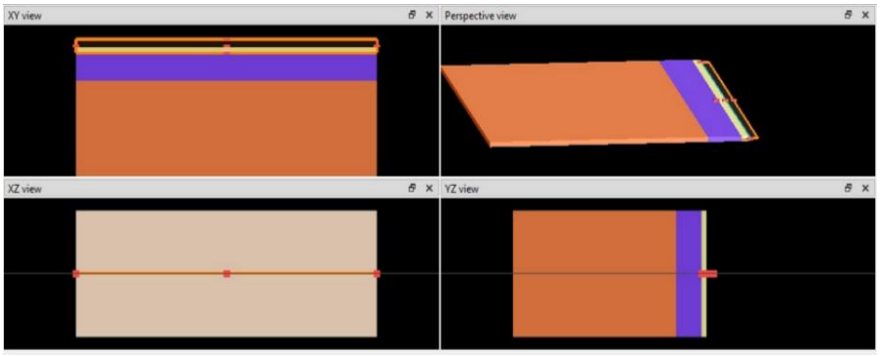

Figure 2. Two dimensions waveguide design using FDE solver.

4. RESULTS AND DISCUSSION

4.1. Single-Layer Test

The sensor characteristics were analyzed and depicted in Figure 3. The resonance wavelength was varied according to the thickness and applied using RI=1, as shown in Figure 3(a). The 30 nm thickness has resonance wavelength values of 650 nm, 710 nm, and 720 nm for Ag, Cu, and Au. The Ag plasmonic material has a significant variation compared to other materials; the resonance wavelength of this plasmonic material shifted from 650 nm to 542 nm. This increased interaction between the incident spectrum in the y-direction with material creasing of thickness, leading to an increased interaction path that leads to a blue shift. The thickness variation with resonance wavelength can be crucial in the waveguide to specify the waveguide efficiency [53-56], as shown in Figure 3(b). The 30 nm thickness has the maximum absorption power at 652.8 nm for silver metal, 728.3 nm for gold metal, and 717.2 nm for copper plasmonic metal. Generally, there is also a loss shift in the plasmonic physics and the wavelength shift, which is the second dependable shift. According to the waveguide structure, increasing the thickness of the metal layer will reduce the loss (reflectivity of the spectrum) at different percentages for the three plasmonic materials. The maximum loss was registered for Au and Ag's minimum loss value. The absorption power substantially affects the sensitivity of plasmonic-based sensors [57-60]. Figure 3(c) shows that FWHM for three plasmonic materials decreases as thickness increases. The absorption is one of the indications for interaction between light and matter, so any increase in thickness leads to increased absorption. The maximum FWHM value was Cu, and the minimum value was Au. 30 nm thickness has the maximum resonance wavelength, loss, and FWHM for all plasmonic materials.

30 nm thickness was the best-verified result according to the characteristics behavior of the single waveguide design. The thickness was tested using RI 1.1, 1.2, and 1.3, as shown in Figure 4, and characterized for FWHM, sensitivity, and Figure of Merits (FOM), as shown in Table 1. In Figure 4, the three materials' blue shift is a dominant feature. However, loss shift has the most significant variation for silver. Moreover, that gives an assertive outcome with both wavelength and loss shift.

The characterizations in Table 1 vary between the maximum values to the minimum values or vice versa. The maximum sensitivity is 112 nm/RIU was registered at Ag 1.2 RI. Furthermore, the lowest value of FWHM was found in Au, which is 34.3. FOM of Au has 0.99295 as the maximum value at 1.3 RI between all tested materials. FOM is generally changed with the analyte's refractive index [61-64].

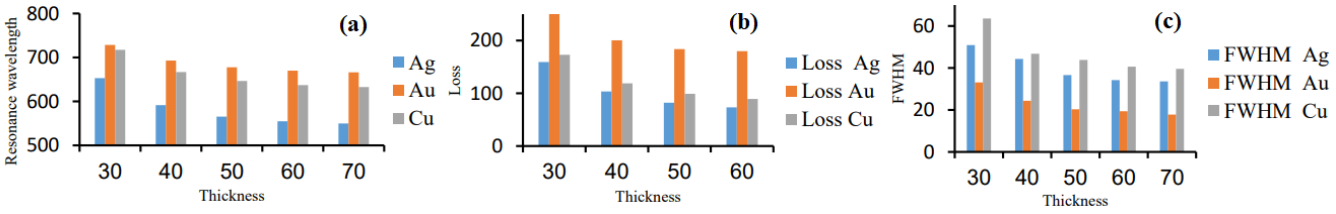

Figure 3. Thickness effect on the a) resonance wavelength b) loss c) FWHM.

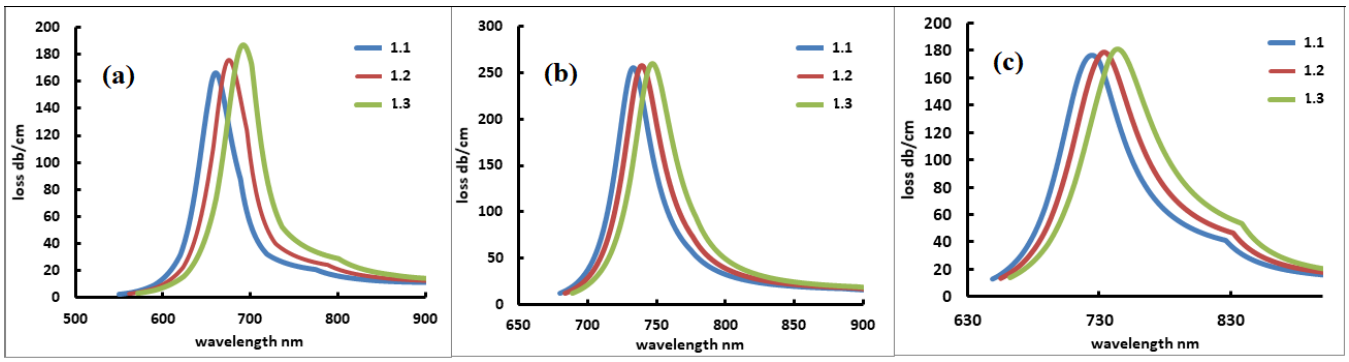

Figure 4. Plasmonic sensor at different refractive indices a) silver metal b) gold metal c) copper metal.

Table 1 Change the refractive index of the analyte with the addition of gold layer 10, 20, and 30nm thick above 30 nm thickness of the gold layer

Thickness	RI	FWHM	Sensitivity nm/RIU	FOM
Ag				
30	1.1	51.9	----	0.453392
30	1.2	48.6	112	0.43392
30	1.3	45	109	0.401785
Au				
30	1.1	34.3	64	0.53593
30	1.2	35.8	58	0.5593
30	1.3	37.2	64	0.58125
Cu				
30	1.1	70	64.9	0.91408
30	1.2	71	67	0.94366
30	1.3	70.5	70.5	0.99295

4.2 Multi-Layer Test

In the multi-layers test, the gold layer was designed theoretically in 10, 20, and 30 nm thickness above the 30 nm of silver and copper separately, as shown in Figure 5. This test was performed under RI =1.1, 1.2, and 1.3 to measure the loss variation, resonance wavelength, sensitivity, FWHM, and FOM.

The quantity of (Figure of merit) is the characterization test for performance for any device. Moreover, it's vital to specify the relative utility of applications [19]. The results in Table 2 (Au/Ag) show significant variation in FOM compared to the single-layer test. The loss value reduced by increasing the thickness; also same behavior was observed in sensitivity. FWHM has stable values almost the same for all thicknesses, but FOM is higher at 30 nm of Au compared to 10 and 20 nm thickness.

The next multi-layer test (Au/Cu) was applied at RI 1.1, 1.2, and 1,3. The gold layer was designed up over copper, as shown in Figure 6. In this Figure, the shift between different refractive indices was recognized. However, their loss values have also changed, supporting plasmonic sensor application.

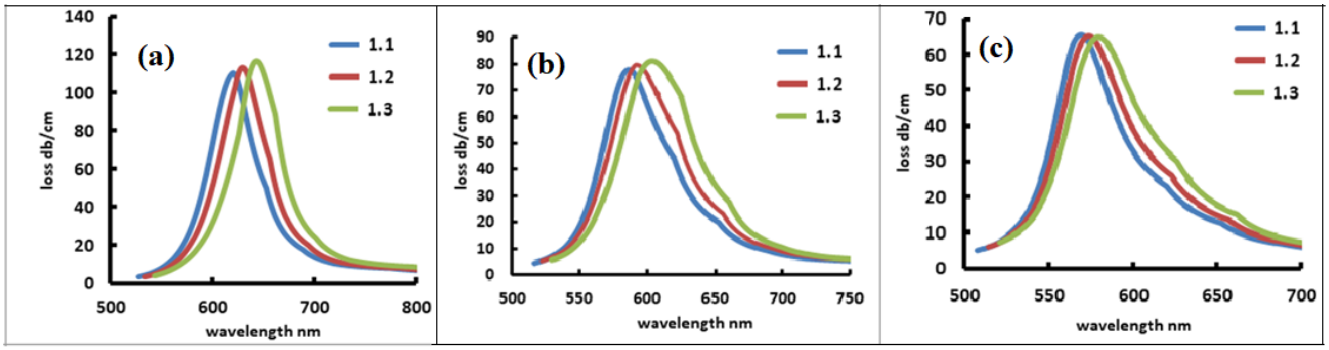

Figure 5. Multi-layer test of (Au/Ag) a) 10 nm/ 30 nm b) 20 nm/ 30 nm c) 30 nm/ 30 nm.

Table 2 Multi-layer test results of Au/Ag

Thickness of the first layer of Ag	Thickness of the second layer Au	RI	Loss	Resonance Wavelength	Sensitivity	FWHM	FOM
30	10	1.1	110.1	619	----	56.1	0.6375
30	10	1.2	113	626.9	88	61.2	0.62613
30	10	1.3	116.5	635.7	83.5	63.1	0.57045
30	20	1.1	77.9	586.5	----	59.9	0.599
30	20	1.2	79.69	591.1	100	61.2	0.612
30	20	1.3	80.97	601.1	73	63.1	0.631
30	30	1.1	65.63	569	----	51.3	1.22142
30	30	1.2	65.18	572.5	42	54.3	1.30238
30	30	1.3	64.69	576.7	38.5	60.9	1.45

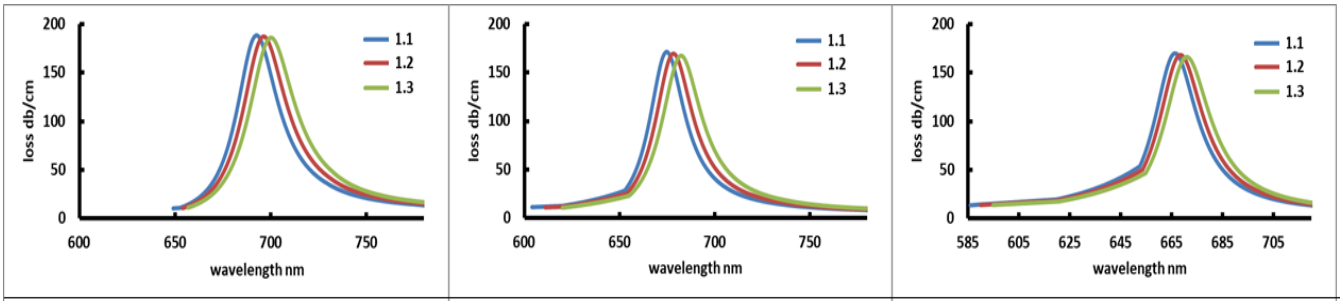

Figure 6. Multi-layer test of (Au/Cu) a) 10 nm/ 30 nm b) 20 nm/ 30 nm c) 30 nm/ 30 nm.

Figure 7 shows the thickness effects of the second gold layer-based above the copper layer. The first three bars represent (10 nm thickness), the second three bars (20 nm thickness), and the last three bars represent (30 nm thickness). In the Figure, reducing loss, FWHM, and sensitivity with increasing RI and gold layer thickness sounds negative. However, the FOM shows a higher value with increasing RI and thickness of the gold layer. The loss value in this type of design is almost stable by variation refractive index from 1.1 to 1.3 for all thicknesses. This design shows low sensitivity between refractive indices at each thickness. Usually, the sensitivity indicates a limit of detection or minimum detectable point.

For the wavelength variation sensing, the sensitivity S_λ and FOM_λ can be calculated according to $S_\lambda = \Delta\lambda/\Delta n$ and $FOM_S = |(\Delta\lambda/\Delta n)/\ FWHM\ |$, respectively, where FWHM is the full width at half maximum of a loss peak. The sensitivity value is not a sufficient calculation because the absolute value of the input parameter magnitude measured is even a crucial factor for a sensor [65-68]

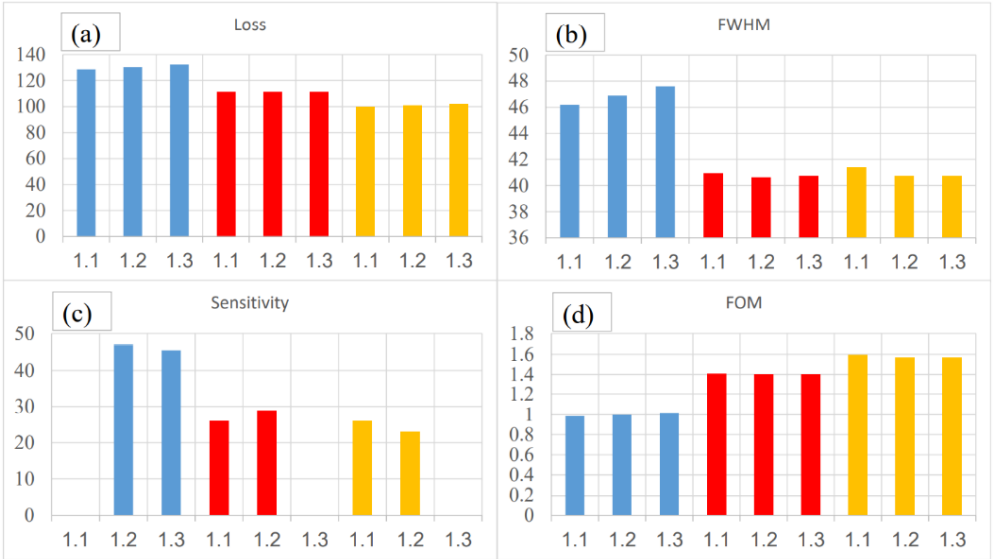

Figure 7. Multi-layer test results of (Au/Cu) a) loss b) FWHM c) sensitivity d) FOM.

4.3 AHP Results

Analytic hierarchy process (AHP) was used to make the calculation process with the AHP method is as follows: In first, create a hierarchical structure of the problem to be solved as shown in Figure 8, then determine the matrix of experimental results as shown in Table 3 by using the equation (6) [69-72]:

$$r = \frac{n(\sum xy) - (\sum x)(\sum y)}{\sqrt{[n\sum x^2 - (\sum x)^2][n\sum y^2 - (\sum y)^2]}} \quad (6)$$

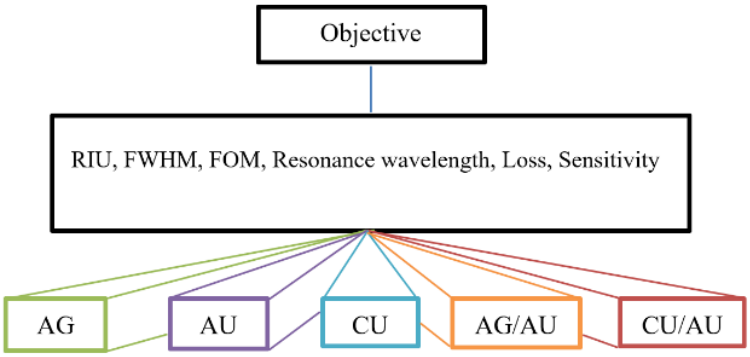

Figure 8. The criteria and the alternatives.

Table 3 Modeling results depicted in matrix

	Thick	Loss	Resonance Wavelength	FWHM	RI	Sensitivity	FOM
Thick	1	0.038772	0.090047699	0.055997	0.181708	0.057194	0.0444
Loss	0.0321	1	0.181708039	0.18761	0.195238	0.004425	0.0332
Wavelength resonance	0.0551	0.0221	1	0.090048	0.055997	0.181708	0.057194
FWHM	0.0643	0.0721	0.0941	1	0.0643	0.0721	0.0941
RI	0.090048	0.055997	0.181708039	0.057194	1	0.0551	0.0221
S	0.181708	0.18761	0.195237571	0.004425	0.0332	1	0.0321
FOM	0.038772	0.090048	0.05599746	0.181708	0.057194	0.0444	1

The matrix comparison in pairs between the criteria was determined as shown in Table 4, calculation of the geometric mean in each value by using the equation (7) as shown in Table (4)

$$GM = \sqrt[n]{X_1 * X_2 * X_3 \dots X_N} \quad (7)$$

Multiplication was performed for the elements in a row and is powered using the equation (8), as shown in Table (5).

$$W_I = \sqrt[n]{a_{11}Xa_{12}X.Xa_{1n}} \quad (8)$$

calculating the priority vector or eigenvector by the weight of each element by using equation (8) as shown in Table (4)

$$X_I = \frac{W_I}{\sum W_I} \quad (9)$$

the result obtained is an Eigenvector (X) as the element weight; after that, the maximum eigenvalue (λmax) was calculated by using the equation (10), as shown in Table (4)

$$\lambda_{max} = \sum a_{ij} * X_i \quad (10)$$

then the consistency index CI was calculated. This calculation is needed to determine the consistency of weights using the following equation as shown in equation (11)

$$C_I = \frac{\lambda_{max} - n}{n - 1} \quad (11)$$

The value consistency ratio was calculated CR when using equation (12) as shown in Table (4)

$$C_R = \frac{C_I}{R_I} \quad (12)$$

Table 4 Calculation of geometric mean for each value

G_{mean}	Weight	A3	A4
0.834	0.171	0.855	5.002
0.851	0.175	0.884	5.063
0.891	0.183	0.912	4.99
0.884	0.181	0.903	4.98
0.788	0.162	0.834	5.158
0.628	0.129	0.638	4.953
4.877	0.113	lam_max	6.22

The consistency index was 0.004 and the consistency ratio 0.0355, which is less than 0.1, which results are accepted to continue in modeling.

The final decision was made based on the normalization results, as shown in Table (5,6). All the alternative matrixes have been constructed through pairwise comparison after examining the experimental results in detail.

Final optimization results show that the best alternative is AU/(priority =93%), as shown in Table (6). The characteristic of the best option was thickness 30 nm, RI= 1.2, loss=257.5, resonance wavelength, 738.3, FWHM= 35.8, sensitivity=64, FOM=0.5593.

Table 5 Criteria applied of waveguide characteristics

	0.1709	0.1746	0.1828	0.1812	0.1617	0.1288	0.113	Priority	Rank
Alternatives	**Thick**	**Loss**	**Resonance wavelength**	**FWHM**	**RI**	**Sensitivity**	**FOM**		
Ag	0.3693	0.3693	0.9163	0.7189	1.4704	0.3269	1.4704	91%	2
Au	0.9163	0.2529	1.0099	0.5301	0.8227	0.4219	0.5757	90%	3
Cu	0.7189	0.3647	1	1	1	0.7174	0.8575	82%	9
Ag	1.4704	0.5757	0.8575	0.7974	1.1844	0.4615	0.7974	85%	5
Au	0.3269	0.8195	0.8106	0.9101	1.0355	0.4635	1.1844	93%	1
Cu	0.5757	1	0.783	0.8246	0.5461	1	0.4615	86%	4
Au/Ag	0.8575	0.3693	0.9163	0.7189	1.4704	0.3269	0.8106	85%	6
Au/Ag	0.7974	0.2529	1.0099	0.5301	0.8227	0.4219	0.783	82%	8
Au/Ag	1.1844	0.3647	1	1	1	0.7174	0.9163	85%	7
Au/Cu	0.4615	0.5757	0.8575	0.7974	1.1844	0.4615	1.0099	86%	5
Au/Cu	0.3693	0.8195	0.8106	0.9101	1.0355	0.4635	0.7189	56%	10
Au/Cu	0.9163	1	0.783	0.8246	0.5461	1	0.7189	33%	11

Table 6 Normalization for priority of matrix A3

	0.1709	0.1746	0.1828	0.1812	0.1617	0.1288	0.113	Priority	Rank
Alternatives	**Thick**	**Loss**	**Resonance wavelength**	**FWHM**	**RI**	**Sensitivity**	**FOM**		
Ag	0.3693	0.3693	0.9163	0.7189	1.4704	0.3269	1.4704	91%	2
Au	0.9163	0.2529	1.0099	0.5301	0.8227	0.4219	0.5757	90%	3
Cu	0.7189	0.3647	1	1	1	0.7174	0.8575	82%	9
Ag	1.4704	0.5757	0.8575	0.7974	1.1844	0.4615	0.7974	85%	5
Au	0.3269	0.8195	0.8106	0.9101	1.0355	0.4635	1.1844	93%	1
Cu	0.5757	1	0.783	0.8246	0.5461	1	0.4615	86%	4
Au/Ag	0.8575	0.3693	0.9163	0.7189	1.4704	0.3269	0.8106	85%	6
Au/Ag	0.7974	0.2529	1.0099	0.5301	0.8227	0.4219	0.783	82%	8

Au/Ag	1.1844	0.3647	1	1	1	0.7174	0.9163	85%	7
Au/Cu	0.4615	0.5757	0.8575	0.7974	1.1844	0.4615	1.0099	86%	5
Au/Cu	0.3693	0.8195	0.8106	0.9101	1.0355	0.4635	0.7189	56%	10
Au/Cu	0.9163	1	0.783	0.8246	0.5461	1	0.7189	33%	11

5. CONCLUSION

Single and multi-layers were investigated using the Finite-difference Eigenmode approach. The highest loss value, FWHM, and FOM were measured at 30 nm thickness for all plasmonic materials in a single layer. Sensitivity, FWHM, and FOM (gold, silver, copper) were characterized at RI= 1.1, 1.2, and 1.3. The maximum sensitivity, FWHM, and FOM were 112 nm/RIU for Ag, 71 copper, and 0.99295 for copper, respectively. In a multi-layer waveguide, the maximum sensitivity was 100 nm/RIU at 30/20 for Ag/Au 1.2 RI, FWHM was found at 63.1 at 30/10 for Au/Ag 1.3 RI, and FOM 1.45 at 30/30 for Ag/Au 1.3 RI. The modeling results for a single layer show that the gold metal has the highest absorption and narrowness of FWHM. The best option was Au rank #1, and priority was 93%, followed by Ag rank #2 at 91% priority. Au/Cu (10/30) thickness rank #5 is the best option and priority 86% in multi-layers results compared to other combinations.

ACKNOWLEDGMENTS

We extend our sincere gratitude and appreciation to everyone who contributed to the support and dissemination of this research, driven by their belief in the importance of advancing scientific knowledge and promoting the research pathway. Your valuable contributions were a fundamental pillar in the success of this work.

REFERENCE

[1] R. C. C. Jorgenson and S. S. S. Yee, "A fiber-optic chemical sensor based on surface plasmon resonance," Sens Actuators B Chem, vol. 12, no. 3, pp. 213–220, 1993, doi: 10.1016/0925-4005(93)80021-3.

[2] Tamara E Abdulrahman, Evan T Salim, Rana O Mahdi and MHA Wahid, Nb2O5 nano and microspheres fabricated by laser ablation, Advances in Natural Sciences: Nanoscience and Nanotechnology, Volume 13, Number4, 045006 (2022), DOI 10.1088/2043-6262/ac99cf.

[3] Fatema H. Rajab, Rana M. Taha, Aseel A. Hadi, Khawla S. Khashan & Rana O. Mahdi , Laser induced hydrothermal growth of ZnO rods for UV detector application, Opt Quant Electron 55, 208 (2023). https://doi.org/10.1007/s11082-022-04473-2

[4] P. Cameron, Optical sensors. 2012.

[5] Jurn Y.N.; Malek F.; Mahmood S.A.; Liu W.-W.; Fakhri M.A.; Salih M.H., Modelling and simulation of rectangular bundle of single-walled carbon nanotubes for antenna applications Key Engineering Materials, 701, 57-66 (2016) 10.4028/www.scientific.net/KEM.701.57.

[6] Azzam Y. Kudhur, Evan T. Salim, Ilker Kara, Makram A. Fakhri & Rana O. Mahdi, Structural optical and morphological properties of copper oxide nanoparticles ablated using pulsed laser ablation in liquid, J Opt 53, 1936–1945 (2024). https://doi.org/10.1007/s12596-023-01331-6.

[7] S. N. Khonina, G. S. Voronkov, E. P. Grakhova, N. L. Kazanskiy, R. V. Kutluyarov, and M. A. Butt, "Polymer Waveguide-Based Optical Sensors—Interest in Bio, Gas, Temperature, and Mechanical Sensing Applications," Coatings, vol. 13, no. 3, p. 549, Mar. 2023, doi: 10.3390/coatings13030549.

[8] Evan T. Salim, Rana O. Mahdi, Doaa Mahmoud, Subash C. B. Gopinath & Forat H. Alsultany, An Analysis Study Employing Laser Ablation in Gold Colloidal at Different Numbers of Laser Pulses, Plasmonics (2025). https://doi.org/10.1007/s11468-025-02998-2.

[9] Hattab F.; Fakhry M., Optical and structure properties for nano titanium oxide thin film prepared by PLD, 2012 1st National Conference for Engineering Sciences, FNCES 2012, 6740474 (2012) 10.1109/NCES.2012.6740474.

[10] M. Bazzan, C. Sada, M. Bazzan, and C. Sada, "Optical waveguides in lithium niobate : Recent developments and applications Optical waveguides in lithium niobate : Recent developments and applications," APPLIED PHYSICS REVIEWS 2, vol. 040603, no. 2(4), pp. 040603–1, 2015, doi: 10.1063/1.4931601.

[11] A. Mahigir and G. Veronis, "Light coupling structures and switches for plasmonic coaxial waveguides," J Appl Phys, vol. 129, no. 19, 2021, doi: 10.1063/5.0043936.

[12] Azzam Y. kudhur, Evan T. Salim, Ilker Kara, Rana O. Mahdi & Raed K. Ibrahim, The effect of laser energy on Cu2O nanoparticles formation by liquid-phase pulsed laser ablation, J Opt 53, 1309–1321 (2024). https://doi.org/10.1007/s12596-023-01319-2.

[13] M. F. O. Hameed and S. Obayya, Computational photonic sensors. 2018. doi: 10.1007/978-3-319-76556-3.

[14] Salim Z.T.; Hashim U.; Arshad M.K.M.; Fakhri M.A., Simulation, fabrication and validation of surface acoustic wave layered sensor based on ZnO/IDT/128° YX LiNBO3, International Journal of Applied Engineering Research, 11(15), 8785-8790 (2016).

[15] Fakhri M.A.; Al-Douri Y.; Hashim U., Fabricated Optical Strip Waveguide of Nanophotonics lthium Niobate, IEEE Photonics Journal, 8(2), 7409919 (2016) 10.1109/JPHOT.2016.2531583.

[16] C. Deleau, H. C. Seat, O. Bernal, and F. Surre, "High-sensitivity integrated SiN rib-waveguide long period grating refractometer," Photonics Res, vol. 10, no. 2, p. 564, Feb. 2022, doi: 10.1364/prj.444825.

[17] Ismail R.A.; Salim E.T.; Hamoudi W.K., Characterization of nanostructured hydroxyapatite prepared by Nd:YAG laser deposition, Materials Science and Engineering C, 33(1), 47-52 (2013) 10.1016/j.msec.2012.08.00.

[18] Abdul Muhsien M.; Salem E.T.; Agool I.R., Preparation and characterization of (Au/n-Sn O2 /Si O2 /Si/Al) MIS device for optoelectronic application, International Journal of Optics, 2013, 756402 (2013) 10.1155/2013/756402.

[19] A. Hasan, R. Al-azawi, and A. Alwahib, "Theory and Modeling of Slab Waveguide Based Surface Plasmon Resonance," Engineering and Technology Journal, vol. 40, no. 8, pp. 1–8, Jul. 2022, doi: 10.30684/etj.2022.132295.1100.

[20] Jurn Y.N.; Malek F.; Mahmood S.A.; Liu W.-W.; Gbashi E.K.; Fakhri M.A., Important parameters analysis of the single-walled carbon nanotubes composite materials, ARPN Journal of Engineering and Applied Sciences, 11(8), 5108-5113 (2016).

[21] Rana O. Mahdi, Aseel A. Hadi, Juhaina M. Taha, Khawla S. Khashan, Preparation of nickel oxide nanoparticles prepared by laser ablation in water, AIP Conf. Proc. 2213, 020309 (2020) https://doi.org/10.1063/5.0000116.

[22] Y. F. Chou Chau et al., "Significantly enhanced coupling effect and gap plasmon resonance in a MIM-cavity based sensing structure," Sci Rep, vol. 11, no. 1, pp. 1–17, 2021, doi: 10.1038/s41598-021-98001-z.

[23] Khawla S. Khashan, Aseel A. Hadi, Rana O. Mahdi & Doaa S. Jubair, Aluminum-doped zinc oxide nanoparticles prepared via nanosecond Nd: YAG laser ablation in water: optoelectronic properties, Opt Quant Electron 56, 125 (2024). https://doi.org/10.1007/s11082-023-05630-x.

[24] Hassan M.A.M.; Al-Kadhemy M.F.H.; Salem E.T., Effect irradiation time of Gamma ray on MSISM (Au/SnO2/SiO2/Si/Al) devices using theoretical modeling, International Journal of Nanoelectronics and Materials, 8(2), 69-82 (2015).

[25] S. Kumar and S. I. Bozhevolnyi, "Single Photon Emitters Coupled to Plasmonic Waveguides: A Review," Adv Quantum Technol, vol. 4, no. 10, pp. 1–14, 2021, doi: 10.1002/qute.202100057.

[26] Fakhri M.A.; Salim E.T.; Wahid M.H.A.; Hashim U.; Salim Z.T.; Ismail R.A., Synthesis and characterization of nanostructured LiNbO3 films with variation of stirring duration, Journal of Materials Science: Materials in Electronics, 28(16), 11813-11822 (2017) 10.1007/s10854-017-6989-0.

[27] Roaa A. Abbas, Evan T. Salim & Rana O. Mahdi, Deposition time effect on copper oxide nano structures, an analysis study using chemical method, J Mater Sci: Mater Electron 35, 427 (2024). https://doi.org/10.1007/s10854-024-12143-0.

[28] S. Nivedha, P. R. Babu, and K. Senthilnathan, "Surface plasmon resonance : physics and technology," Curr Sci, vol. 115, no. 1, 2018.

[29] Fakhri M.A.; Wahid M.H.A.; Badr B.A.; Kadhim S.M.; Salim E.T.; Hashim U.; Salim Z.T., Enhancement of Lithium Niobate nanophotonic structures via spin-coating technique for optical waveguides application, EPJ Web of Conferences, 162, 1004 (2017) 10.1051/epjconf/201716201004.

[30] Evan T. Salim, Rana O. Mahdi, Tamara E. Abdulrahman, Makram A. Fakhri, Jehan A. Siamon, Ahmad S. Azzahrani & Subash C.B. Gopinath, RE-crystallization of Nb2O5 nanocrystals: a study employing different laser wavelength, J Opt (2024). https://doi.org/10.1007/s12596-024-01942-7.

[31] M. A. Fakhri, M. J. AbdulRazzaq, A. A. Alwahib, and W. H. Muttlak, "Theoretical study of a pure LinbO3/Quartz waveguide coated gold nanorods using supercontinuum laser source," Opt Mater (Amst), vol. 109, 2020, doi: 10.1016/j.optmat.2020.110363.

[32] Fakhri M.A.; Salim E.T.; Wahid M.H.A.; Hashim U.; Salim Z.T., Optical investigations and optical constant of nano lithium niobate deposited by spray pyrolysis technique with injection of Li2CO3 and Nb2O5 as raw materials, Journal of Materials Science: Materials in Electronics, 29(11), 9200-9208 (2018) 10.1007/s10854-018-8948-9.

[33] Salim E.T.; Saimon J.A.; Abood M.K.; Fakhri M.A., Some physical properties of Nb2O5 thin films prepared using nobic acid based colloidal suspension at room temperature, Materials Research Express, 4(10), 106407 (2017) 10.1088/2053-1591/aa90a6.

[34] R. D. Harris and J. S. Wilkinson, "Waveguide surface plasmon resonance sensors," Sens Actuators B Chem, vol. 29, no. 1–3, pp. 261–267, 1995, doi: 10.1016/0925-4005(95)01692-9.

[35] B. H. Ong, X. Yuan, and S. C. Tjin, "Bimetallic silver-gold film waveguide surface plasmon resonance sensor," Fiber and Integrated Optics, vol. 26, no. 4, pp. 229–240, 2007, doi: 10.1080/01468030701347106.

[36] S. K. Mishra, B. Zou, and K. S. Chiang, "Surface-Plasmon-Resonance Refractive-Index Sensor with Cu-Coated Polymer Waveguide," IEEE Photonics Technology Letters, vol. 28, no. 17, pp. 1835–1838, 2016, doi: 10.1109/LPT.2016.2573322.

[37] M. S. Aruna Gandhi and Q. Li, "Grooved Gold Grating-Assisted Integrated Planar Waveguide Based Localized Surface Plasmon Polariton Microbiosensor," 2020 5th Optoelectronics Global Conference, OGC 2020, no. September, pp. 193–196, 2020, doi: 10.1109/OGC50007.2020.9260467.

[38] L. Ji, S. Yang, R. Shi, Y. Fu, J. Su, and C. Wu, "Polymer Waveguide Coupled Surface Plasmon Refractive Index Sensor: A Theoretical Study," Photonic Sensors, vol. 10, no. 4, pp. 353–363, 2020, doi: 10.1007/s13320-020-0589-y.

[39] D. Pandey and V. Kushwaha, "The use of Analytical Hierarchy Process in sensor-based networks for security-aware congestion control," Networks and Heterogeneous Media, vol. 18, no. 1, 2023, doi: 10.3934/nhm.2023009.

[40] S. Ol and A. Momani, "Selection of temperature measuring sensors using the analytic hierarchy process," 2011. [Online]. Available: https://orb.binghamton.edu/systems_students.

[41] A. Frikha and H. Moalla, "Analytic hierarchy process for multi-sensor data fusion based on belief function theory," Eur J Oper Res, vol. 241, no. 1, 2015, doi: 10.1016/j.ejor.2014.08.024.

[42] D. Diakoulaki, G. Mavrotas, and L. Papayannakis, "Determining objective weights in multiple criteria problems: The critic method," Comput Oper Res, vol. 22, no. 7, pp. 763–770, 1995, doi: 10.1016/0305-0548(94)00059-H.

[43] Evan T. Salim, Ahmed T. Hassan, Rana O Mahdi, Forat H. Alsultany, Physical Properties of HfO2 Nano Structures Deposited using PLD, IJNeaM, vol. 16, no. 3, pp. 495–510, Oct. 2023.

[44] Fakhri M.A.; Numan N.H.; Mohammed Q.Q.; Abdulla M.S.; Hassan O.S.; Abduljabar S.A.; Ahmed A.A., Responsivity and response time of nano silver oxide on silicon heterojunction detector, International Journal of Nanoelectronics and Materials, 11(Special Issue BOND21), 109-114 (2018).

[45] Aseel A. Hadi, Juhaina M. Taha, Rana O. Mahdi, Khawla S. Khashan, Influence of laser pulse on properties of NiO NPs prepared by laser ablation in liquid, AIP Conf. Proc. 2213, 020308 (2020) https://doi.org/10.1063/5.0000115.

[46] M. Žižovic, B. Miljkovic, and D. Marinkovic, "Objective methods for determining criteria weight coefficients:a modificationof the critic method," Decision Making: Applications in Management and Engineering, vol. 3, no. 2, pp. 149–161, 2020, doi: 10.31181/dmame2003149z.

[47] Roaa A. Abbas, Evan T. Salim, and Rana O. Mahdi, Study based on micro-and nanosized raw materials using the hydrothermal method, International Journal of Nanoelectronics and Materials (IJNeaM)Volume 18, No. 1, January 2025 [141-149]. https://doi.org/10.58915/ijneam.v18i1.1751.

[48] Fakhri M.A.; Al-Douri Y.; Bouhemadou A.; Ameri M., Structural and Optical Properties of Nanophotonic LiNbO3 under Stirrer Time Effect, Journal of Optical Communications, 39(3), 297-306 (2018) 10.1515/joc-2016-0159.

[49] Zainab T. Hussain, Khawla S. Khashan, Rana O. Mahdi, Characterization of cadmium oxide nanoparticles prepared through Nd:YAG laser ablation process, Materials Today: ProceedingsVolume 42, Pages 2645 – 26482021. https://doi.org/10.1016/j.matpr.2020.12.594.

[50] T. A.- Pachemska, M. Lapevski, and R. Timovski, "Analytical Hierarchical Process (AHP) method application in the process of selection and evaluation," Proceedings. Gabrovo: Internatinal Scientific Conference "UNITECH". 21-22 November 2014, no. November, pp. 373–380, 2014.

[51] Fakhri M.A.; Wahid M.H.A.; Kadhim S.M.; Badr B.A.; Salim E.T.; Hashim U.; Salim Z.T., The structure and optical properties of Lithium Niobate grown on quartz for photonics application, EPJ Web of Conferences, 162, 1005 (2017) 10.1051/epjconf/201716201005.

[52] Abdul Amir H.A.A.; Fakhri M.A.; Abdulkhaleq Alwahib A., Review of GaN optical device characteristics, applications, and optical analysis technology, Materials Today: Proceedings, 42, 2815-2821 (2021) 10.1016/j.matpr.2020.12.727.

[53] M. A. Fakhri, E. T. Salim, M. H. A. Wahid, A. W. Abdulwahhab, U. Hashim, and Z. T. Salim, "Efficiency enhancement of optical strip waveguide by the effect of heat treatment," Optik (Stuttg), vol. 180, no. December 2018, pp. 768–774, 2019, doi: 10.1016/j.ijleo.2018.12.006.

[54] Abdul Amir H.A.A.; Fakhri M.A.; Alwahib A.A.; Salim E.T., Optical Investigations of GaN Deposited Nano Films Using Pulsed Laser Ablation in Ethanol, International Journal of Nanoelectronics and Materials, 15(2), 129-138 (2022).

[55] Jabbar H.D.; Fakhri M.A.; AbdulRazzaq M.J., Synthesis Gallium Nitride on Porous Silicon Nano-Structure for Optoelectronics Devices, Silicon, 14(18) 12837-12853 (2022) 10.1007/s12633-022-01999-8.

[56] Abdul Amir H.A.A.; Fakhri M.A.; Alwahib A.A.; Salim E.T.; Alsultany F.H.; Hashim U., Synthesis of gallium nitride nanostructure using pulsed laser ablation in liquid for photoelectric detector, Materials Science in Semiconductor Processing, 150, 106911 (2022) 10.1016/j.mssp.2022.106911.

[57] A. Abdulkhaleq Alwahib, S. Fawzi Alhasan, M. H. Yaacob, H. N. Lim, and M. Adzir Mahdi, "Surface plasmon resonance sensor based on D-shaped optical fiber using fiberbench rotating wave plate for sensing pb ions," Optik (Stuttg), vol. 202, 2020, doi: 10.1016/j.ijleo.2019.163724.

[58] Evan T. Salim, Roaa A. Abbas, Raed K. Ibrahim, Rana O. Mahdi, Makram A. Fakhri, Ahmad S. Azzahrani, Forat H. Alsultany, Subash C. B. Gopinath & Zaid T. Salim, Impact of Decoration Method on Some Physical Properties of Ag@Cu2O Nanostructure, Plasmonics (2024). https://doi.org/10.1007/s11468-024-02569-x.

[59] Fakhri M.A.; Wahid M.H.A.; Kadhim S.M.; Badr B.A.; Salim E.T.; Hashim U.; Salim Z.T., The structure and optical properties of Lithium Niobate grown on quartz for photonics application, EPJ Web of Conferences, 162, 1005 (2017) 10.1051/epjconf/201716201005.

[60] Khawla S khashan, Rana O Mahdi, Ban A. Badr, Farah Mahdi, Preparation and characterization of ZnMgO nanostructured materials as a photodetector, Journal of Physics: Conference Series 1795 (2021) 012008. doi:10.1088/1742-6596/1795/1/012008.

[61] M. Tian, P. Lu, L. Chen, C. Lv, and D. Liu, "All-solid D-shaped photonic fiber sensor based on surface plasmon resonance," Opt Commun, vol. 285, no. 6, pp. 1550–1554, Mar. 2012, doi: 10.1016/j.optcom.2011.11.104.

[62] Jabbar H.D.; Fakhri M.A.; Jalal Abdulrazzaq M., Gallium Nitride -Based Photodiode: A review, Materials Today: Proceedings, 42, 2829-2834 (2021) 10.1016/j.matpr.2020.12.729.

[63] Roaa A. Abbas, Evan T. Salim & Rana O. Mahdi, Morphology transformation of Cu2O thin film: different environmental temperatures employing chemical method, J Mater Sci: Mater Electron 35, 1057 (2024). https://doi.org/10.1007/s10854-024-12823-x.

[64] Fakhri, Makram A., Salim, Evan T., Ketab, Marwah R., Jabbar, Haneen D., Ibrahim, Omar A., Azzahrani, Ahmad S., AbdulRazzaq, Mohammed Jalal, Ismail, Raid A., Basem, Ali, Alsultany, Forat H. Gopinath, Subash C. B., Optimizing charge transport in hybrid GaN-PEDOT:PSS/PMMADevice for advanced application, Scientific Reports14(1), 12841 (2024).

[65] X. Y. Wang et al., "Lasing Enhanced Surface Plasmon Resonance Sensing," Nanophotonics, vol. 6, no. 2, pp. 472–478, 2017, doi: 10.1515/nanoph-2016-0006.

[66] Abdul Amir H.A.A.; Fakhri M.A.; A.Alwahib A.; Salim E.T.; Alsultany F.H.; Hashim U., An investigation on GaN/ porous-Si NO2 gas sensor fabricated by pulsed laser ablation in liquid, Sensors and Actuators B: Chemical, 367, 132163 (2022) 10.1016/j.snb.2022.132163.

[67] Salim E.T.; Halboos H.T., Synthesis and physical properties of Ag doped niobium pentoxide thin films for Ag-Nb2O5/Si heterojunction device, Materials Research Express, 6(6), 66401 (2019) 10.1088/2053-1591/ab07d3.

[68] A. A. Alwahib, Y. M. Kamil, M. H. A. Bakar, M. A. Mahdi, and F. H. Suhailin, "Optical Detection of Lead Ion with Surface Plasmon Resonance Configurations," in 2020 IEEE 8th International Conference on Photonics, ICP 2020, 2020. doi: 10.1109/ICP46580.2020.9206481.

[69] Alsultany F.H.; Alhasan S.F.H.; Salim E.T., Seed Layer-Assisted Chemical Bath Deposition of Cu2O Nanoparticles on ITO-Coated Glass Substrates with Tunable Morphology, Crystallinity, and Optical Properties, Journal of Inorganic and Organometallic Polymers and Materials, 31(9), 3749-3759 (2021) 10.1007/s10904-021-02016-y.

[70] Doaa A. Mahmoud, Evan T. Salim, Rana O. Mahdi, A. Mindil, Subash C. B. Gopinath & Motahher A. Qaeed, Laser Ablation of Tungsten Metal for Au@WO3 Core-Shell Formation: A Characterizing Study at Different Laser Fluences, Plasmonics (2024). https://doi.org/10.1007/s11468-024-02607-8.

[71] Ismail R.A.; Salim E.T.; Halbos H.T., Preparation of Nb2O5 nanoflakes by hydrothermal route for photodetection applications: The role of deposition time, Optik, 245, 167778 (2021) 10.1016/j.ijleo.2021.167778.

[72] Alwazny M.S.; Ismail R.A.; Salim E.T., Aggregation threshold for Novel Au – LiNbO3 core/shell Nano composite: effect of laser ablation energy fluence, International Journal of Nanoelectronics and Materials, 15(3), 223-232 (2022).